frontiers | Frontiers in Energy Research

TYPE Brief Research Report
PUBLISHED 28 July 2023
DOI 10.3389/fenrg.2023.1205704

OPEN ACCESS

EDITED BY
Tao Zhang,
Shanghai University of Electric Power, China

REVIEWED BY
Haifei Chen,
Changzhou University, China
Lokesh Varshney,
Galgotias University, India

*CORRESPONDENCE
Ch. Rami Reddy,
crreddy229@gmail.com
Muhammad Khalid,
mkhalid@kfupm.edu.sa

RECEIVED 14 April 2023
ACCEPTED 29 June 2023
PUBLISHED 28 July 2023

CITATION
Kumar Kolluru A, Malligunta KK, Teja SR, Reddy CR, Alqahtani M and Khalid M (2023), A novel controller for PV-fed water pumping optimization system driven by an 8/6 pole SRM with asymmetrical converter.
Front. Energy Res. 11:1205704.
doi: 10.3389/fenrg.2023.1205704

A novel controller for PV-fed water pumping optimization system driven by an 8/6 pole SRM with asymmetrical converter

Ashok Kumar Kolluru[1], Kiran Kumar Malligunta[1], S. Ravi Teja[1], Ch. Rami Reddy[2]*, Mohammed Alqahtani[3] and Muhammad Khalid[4,5,6]*

[1]Department of Electrical and Electronics Engineering, Koneru Lakshmaiah Education Foundation, Guntur, Andhra Pradesh, India, [2]Department of Electrical and Electronics Engineering, Joginpally B. R. Engineering College, Hyderabad, India, [3]Department of Industrial Engineering, King Khalid University, Abha, Saudi Arabia, [4]Electrical Engineering Department, King Fahd University of Petroleum and Minerals, Dhahran, Saudi Arabia, [5]Interdisciplinary Research Center for Renewable Energy and Power Systems (IRC-REPS), King Fahd University of Petroleum and Minerals, Dhahran, Saudi Arabia, [6]SDAIA-KFUPM Joint Research Center for Artificial Intelligence, King Fahd University of Petroleum and Minerals, Dhahran, Saudi Arabia

A locally installed photovoltaic (PV)-powered motor pump is a viable solution for a water pumping system (WPS) in rural locations. In this study, a single-stage, PV-fed, SRM-powered WPS was investigated and realized using a speed sensorless sliding mode controller (SMC)-based direct torque control (DTC). As a result, no additional DC-DC converter was required for maximum power absorption from the PV source. By utilizing a novel high-side switch asymmetric converter with a hybrid Perturb and Observe–Grey Wolf optimization (POGWO) method integrated with a DC-link voltage controller, an efficient single-stage conversion was achieved. The robustness of the proposed integrated control is presented by comparing it with a Genetic Algorithm and Particle Swarm Optimization (PSO). Extensive results using MATLAB SIMULINK are shown to validate the proposed system in both steady-state and transient conditions for various partial shading conditions.

KEYWORDS

solar PV system, switched reluctance motor, asymmetrical converter, direct torque control, sliding mode controller

1 Introduction

In India, there are an estimated 21 million irrigation pumps, of which more than 9 million are powered by diesel generators and the rest by the main electrical grid (Narale and Singh Rathore, 2015). Photovoltaic (PV)-based water pumping systems (WPS) are gradually gaining popularity in several countries. Battery-free PV-based WPS is a cost-effective and reliable alternative (Thumu et al., 2021). To achieve optimal PV module usage, a maximum power point tracking (MPPT) device with a suitable algorithm is necessary to produce maximum power output from the PV system. However, the system's design and dimensions will increase if a second device is added to track the maximum power. As a result, stand-alone PV-fed WPSs can offer a low-cost alternative with a small footprint (Goud and Reddy, 2020; Thumu et al., 2021). Among the many motors available on the

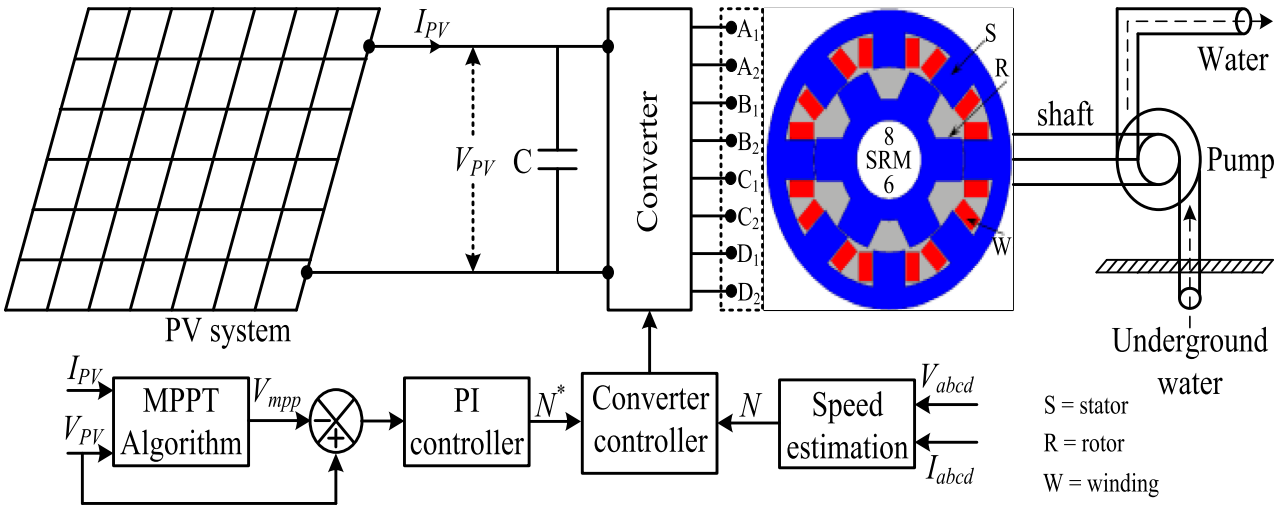

FIGURE 1
Proposed water pumping system.

TABLE 1 PV module Specifications (Rajanna and Kumar, 2021).

S.No	Specifications	Value
1	V_{oc}	48.50 V
2	I_{sc}	8.16 A
3	V_{MPP}	39.60 V
4	I_{MPP}	7.66 A
5	P_{max}	302 W
6	Number of series modules	16no's

market, switch reluctance motors (SRMs) are the best choice for driving the pump that lifts water from great depths.Since producing large torque motors is necessary to lift water from great depths, an 8/6 pole motor for WPS is considered in this work. PV-based WPSs with different kinds of AC motors have been proposed by many researchers. The authors in (Abido et al., 2015; Jayachandran et al., 2021) proposed a WPS in which an induction motor (IM) drives the pump. The authors in (Kumar and Singh, 2017) suggested that a differential technique for maximum power point tracking used in a WPS was also used in conjunction with a synchronous reluctance motor for partially shaded conditions. In (Mishra et al., 2020), a permanent magnet synchronous motor with hybrid proportional integral control for solar-assisted WPS was proposed, in which there is pre-compensation of errors using fuzzy logic. The authors in (Shukla and Singh, 2019) presented a grid-connected PV-assisted power supply system for WPS in which machine learning is employed for sensorless control of the induction motor. This also has the advantage of power export to the grid under load-free conditions. The authors of (Ibrahim et al., 2019; Murshid and Singh, 2019) described a grid-connected WPS powered by a synchronous reluctance motor and using the same inverter to enhance the quality of grid power, while in (Kumar and Singh, 2019; Shukla and Singh, 2020) BLDC was utilized for WPS. SRMs are the most ideal for WPS, especially in single-stage PV-fed systems, due to their advantages over other motors (Mishra and Singh, 2018).

Many strategies for Maximum Power Point Tracking (MPPT) are known and have been applied. In addition, due to its simplicity and efficiency, the Perturb and Observe (P&O) approach has attracted the attention of many researchers for hybridizing this algorithm (Ramulu et al., 2018; Pradhan et al., 2020). A PV system consists of multiple PV modules that are connected in series and parallel, with each module containing a large number of PV cells. The authors of (Khalid and Savkin, 2010; Sundareswaran et al., 2015) proposed a distributed MPPT technique that utilized several converters to improve conversion efficiency. The cost and size of such a system is bound to increase The utilization of Grey Wolf Optimization (Mohanty et al., 2017) and Genetic Algorithm (Malla and N Bhende, 2014) for MPPT has been observed to improve the efficiency and accuracy of MPPT. Novel circuit topologies and machines (Manne et al., 2020; Rajanna and Kumar, 2021) have been proposed to reduce the complexity of the interface. Reduced switching converters (Kolluru and Kumar, 2021) and the integration of DC stages (Shanthi et al., 2021) have been proven to reduce overall components. Variety of control strategies for closed-loop control of motors such as vector control (Murshid and Singh, 2018), direct torque control (DTC) (Yan et al., 2019), improved DTC (Sir et al., 2020), intelligent controller (Varshney et al., 2021), model reference adaptive control (MRAC) (Haq et al., 2023; Kashif and Singh, 2023), peak current detection-based control (Sen and Singh, 2021) and fuzzy logic controller (FLC) (Stonier et al., 2021; Ríos-Castro et al., 2023) of which few are mathematical approach and rest are heuristic approach both of which proved dominance in certain control parameters.

To develop an efficient, reliable, and cost-effective water pumping system, a high-side switch asymmetrical converter was built using a single-stage WPS fed by PV and powered by a sliding mode controller (SMC)-based speed sensorless direct torque control

10.3389/fenrg.2023.1205704

TABLE 2 Accounting for partial shading in the PV array.

Pattern	Irradiance level of modules in each array
PSC-1	Modules 1–4: 1,000 W/m^2, Modules 5–8: 900 W/m^2, Modules 9–12: 800 W/m^2, Modules 13–16: 700 W/m^2
PSC-2	Modules 1–3: 1,000 W/m^2, Modules 4–7: 950 W/m^2, Modules 8–13: 700 W/m^2, Modules 14–16: 550 W/m^2
PSC-3	Module 1: 800 W/m^2, Modules 2–4: 700 W/m^2, Modules 5–11: 550 W/m^2, Modules 12–16: 300 W/m^2

(DTC). The following novel contributions to the WPS are presented in this paper.

- An asymmetrical bridge converter with a common high-side switch, which reduced the number of switches, with the power conversion equivalent to that of a conventional asymmetrical bridge converter.
- A proposed single-stage conversion of PV power using the same drive converter for tracking the maximum power and eliminating the need for an additional MPPT DC-DC converter.
- A control structure for the drive converter that was modified with an additional objective to include MPP control along with drive current control.
- A model-based estimation of motor speed, employed in the control to eliminate the need for a speed-sensing unit, which otherwise would have added to the cost of the drive. However, this solution also makes submersible pumping more difficult to implement.
- An adaptive direct torque control, which was adopted for the current control of robustness under variations of head and pressure conditions.

The rest of the paper is organized as follows. Section 2 presents the topology and mathematical model of the proposed system. Section 3 presents the control structure. Section 4 presents the simulation results, and Section 5 presents the conclusions.

2 System description

The suggested WPS is comprised of a PV system for power supply and a converter that drives the motor and also serves as an MPPT converter, as shown in Figure 1. MRAC was used to build a sensorless speed controller (SPC), and SMC was designed to monitor the speed at its rated value, which was generated by DC link control (DCLC), to address this issue. The component modeling and design are provided below.

To avoid the frictional force of the rotating elements involved in lifting the water motor/pump breakaway, the torque (T_b) must be between 10% and 25% of the nominal torque. Whenever the speed exceeds a certain threshold or base value (ω_t), the pump starts pumping water. The rate of water flow "Q" (gallons per minute) fluctuates proportionally with the speed, head, horsepower, and brake horsepower as indicated in Eqs 1–4 (Pradhan et al., 2020).

$$Q = \begin{cases} a\omega - b & \omega \geq \omega_t \\ 0 & \omega < \omega_t \end{cases} \tag{1}$$

$$H = a_0\omega^2 + a_1\omega Q + a_2 Q^2 \tag{2}$$

The motor's desired horsepower capacity is calculated as:

$$W_{hp} = \frac{Q \times H}{3960} \tag{3}$$

The real power required to run the pump should be greater than W_{hp} due to its efficiency. The Horsepower is defined as the Horsepower necessary for the pump shaft to pump a given flow rate against a given H is calculated as:

$$BHP = W_{hp} / \left(\eta_p * \eta_d\right) \tag{4}$$

It is assumed that Q_{max} is 150 gallons per minute, H is 50 m, the pump efficiency (η_p) is 1, and the drive efficiency (η_d) is 0.95. The solar panel power availability will be approximately 1900 W, assuming a minimum irradiance availability of 400 W/m^2. The minimum motor speed is set at 720 rpm according to the minimum power of the solar panel, and the maximum speed is obtained at 1800 rpm.

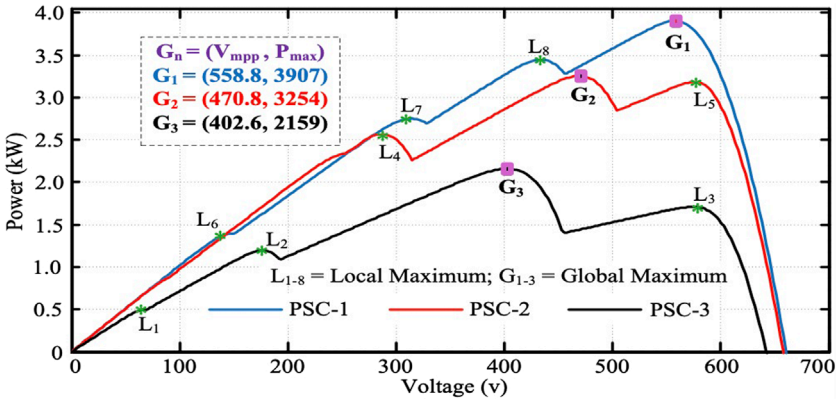

FIGURE 2
P-V characteristics for one string under partial shading.

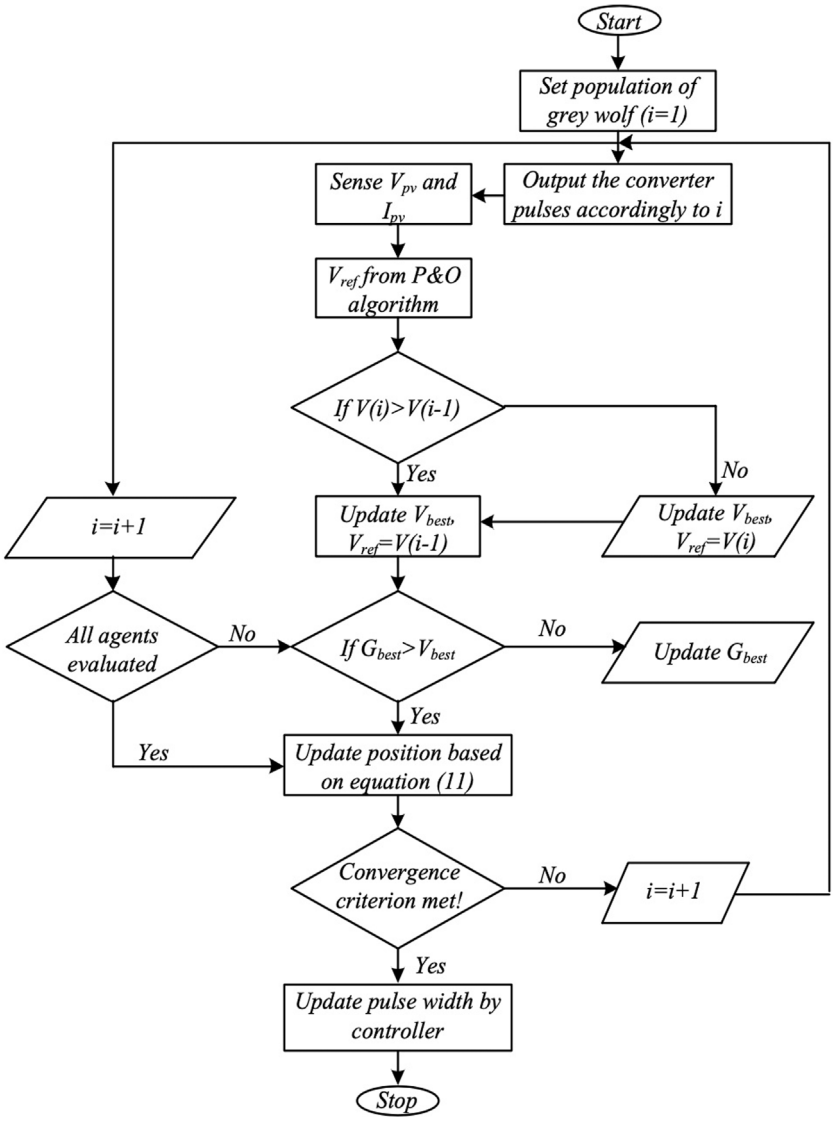

FIGURE 3
GWO-based MPPT algorithm.

The maximum speed and maximum power are used to compute the motor load, T_L = 25 Nm. Furthermore, the frictional force between the pipe and the water will increase the load torque on the motor. Additionally, if an extra pipe is constructed to transport water to a different location for use, the load torque will increase.

2.1 Modeling of the SRM system

Generally, reluctance machines consist of variable reluctance magnetic circuits in both the rotor and stator, or they are double salient machines. The following equations (Abido et al., 2015; Kumar and Singh, 2017; Ibrahim et al., 2019; Shukla and Singh, 2019; Mishra et al., 2020) are used to model the motor (Ramulu et al., 2018).

The flux linkage for applied stator voltage can be expressed as

$$V = \frac{(\lambda_a - \lambda_u)i}{\lambda_u} = \frac{(L_a^s - L_u)i}{t} \tag{5}$$

where $t = \frac{\beta_s}{\omega_r}$, $\sigma_s = \frac{L_a^s}{L_a}$ and $\sigma_u = \frac{L_u^s}{L_u}$

In terms of rotor speed, the rate of flux change is expressed as

$$V = \frac{\omega_r}{\beta_s} L_a^s i\left(1 - \frac{1}{\sigma_s \sigma_u}\right) \tag{6}$$

Now, this $L^s{}_a\ i$ product would be transformed into machine physical parameters as

$$L_a^s i = \varphi T_{ph} = B \times A_{sp} \times T_{ph} = B \times D \times L \times \beta_s \times T_{ph}/2 \tag{7}$$

where $A_s = \frac{2T_{ph}im}{\pi D}$

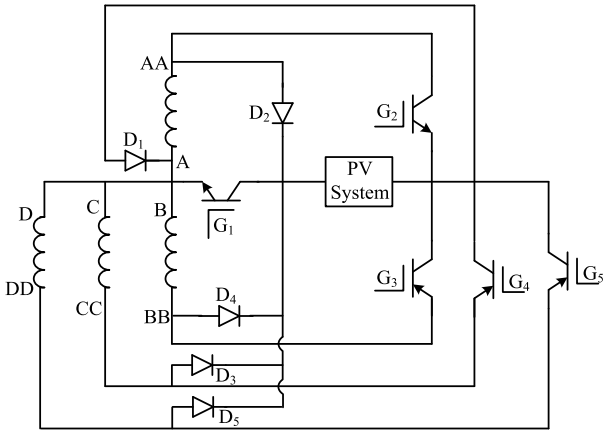

FIGURE 4
Modified converter with a reduced number of switches.

However, the power depends on the input voltage and can be expressed by

$$P_d = K_a K_d V_{in}$$

$$P_d = k_d k_e \left(\frac{\pi^2}{120}\right)\left(1 - \frac{1}{\sigma_s \sigma_u}\right) BA_s D^2 L N_r \tag{8}$$

Finally, the electromagnetic torque produced by a motor is given by the expression

$$T = k_d k_e k_3 k_2 (BA_s) D^2 L \tag{9}$$

where $k_d = \frac{\theta_i q P_r}{360}$, $k_2 = 1 - \frac{1}{\sigma_s \sigma_u}$, $k_3 = \frac{\pi}{4}$

L_a^s and L_u are aligned and unaligned inductances (per phase), respectively. t is the time required for the rotor to go from aligned to unaligned. β_s is the stator pole arc, L_a^u is the aligned unsaturated inductance, φ is the aligned flux, and Asp is the stator pole area. D is the stator bore diameter, and L is the stator bore length. B is the flux density of the stator poles, and T_{ph} represents the turns per pole. m is the number of simultaneously conducting phases. k_d is the duty cycle, θ_i is the current conducted per phase. P_s is the number of stator poles, and P_r is the number of rotor poles.

The electromagnetic torque generated by the motor is required to drive the load torque due to the water pump and causes due to friction between pipe water Hence, the load torque (T_L = 25) and the electromagnetic torque can be expressed as

$$T_e = j\frac{d\omega}{dt} + B\omega + 25 \tag{10}$$

2.2 PV system

To achieve the required maximum power of 4800 W, 16 PV modules of 302 W each were chosen. Table 1 shows a comprehensive list of PV module specifications.

The required DC voltage level and power are generated by connecting 16 PV modules in series. The voltage corresponding to the Maximum Power Point (MPP) for uniform solar irradiation can be monitored using the standard P&O techniques, as illustrated below:

$$V_{mpp}(i+1) = V_{mpp}(i) + \Delta V \times sign\left(\frac{dP_{pv}}{dV_{pv}}\right) \tag{11}$$

The PV array consists of 16 serial modules connected in series to generate the required voltage. The P-V characteristics for different partial shading conditions as depicted in Table 2 are shown in Figure 2.

The Grey Wolf Optimization algorithm is a new metaheuristic optimization technique. The basic principle is to imitate grey wolves as they hunt in a cooperative way. The most popular metaheuristic optimization techniques are GA (Pourfarrokh et al., 2023), ACO (Li et al., 2023), GSA (Kumaraswamy et al., 2023), PSO (Abubakar et al., 2023), etc. These techniques are generally used in the domain of power systems, but they have also spread to other areas of research. The advantages of these algorithms are flexibility, simplicity, freedom from derivations, and avoidance of local optima. Even though the conventional algorithms are inspired by nature and randomly initialized, they suffer from poor convergence rates, more computation time, and large dimensions, and there is no guarantee of a global solution for optimization. Hence, the Grey Wolf Optimization algorithm has been proposed, which has a higher chance of improvement in identifying the global maximum of PV power during partial shading conditions.

The global best position of the voltage corresponding to the maximum power can be obtained from Eq. **12**. The corresponding flowchart of the GWO-based MPPT algorithm under partial shading conditions is depicted in Figure 3.

$$\vec{V}_{(i+1)} = \frac{\vec{V}_1 + \vec{V}_2 + \vec{V}_3}{3} \tag{12}$$

so that

$$V_1 = V_\alpha - A_1(D_\alpha);\ V_2 = V_\beta - A_2(D_\beta);\ V_3 = V_\delta - A_3(D_\delta) \tag{13}$$

$$D_\alpha = \left|C_1 V_\alpha - V_{pv}\right|;\ D_\beta = \left|C_2 V_\beta - V_{pv}\right|;\ D_\delta = \left|C_3 V_\delta - V_{pv}\right| \tag{14}$$

$$\vec{A} = 2\vec{a}\vec{r}_1 - \vec{a};\ \vec{C} = 2\vec{r}_2 \tag{15}$$

where the components of "a" are linearly decreased from 2 to 0. Similarly, r_1 and r_2 are randomly varied in the range [0, 1].

2.3 High side switch asymmetric converter

The conventional converter to run an 8/6 pole SRM has eight switches (de Oliveira et al., 2023; Sagvand et al., 2023).

TABLE 3 Required switching pattern.

S. No	Angle	Switching
1	0 to 90	(1, 1, 1, 0, 0)/(1, 0, 0, 0, 1)
2	90 to 180	(1, 0, 1, 1, 0)/(0, 1, 0, 0, 0)
3	180 to 270	(1, 0, 0, 1, 1)/(1, 0, 1, 0, 1)
4	270 to 360	(1, 1, 0, 0, 1)/(1, 0, 0, 1, 0)

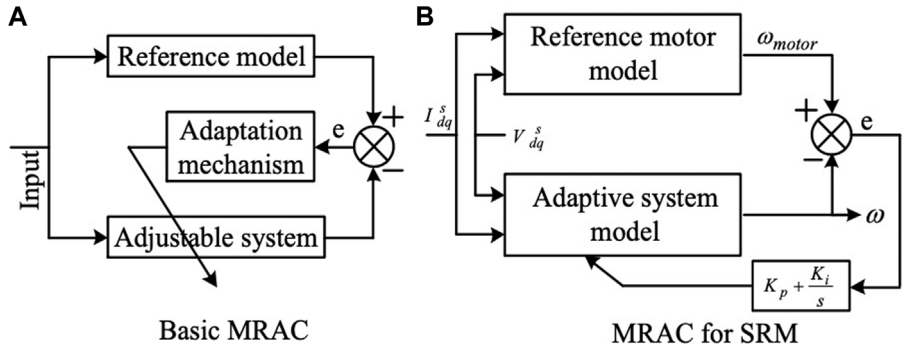

FIGURE 5
Speed estimation using SRM's MRAC model.

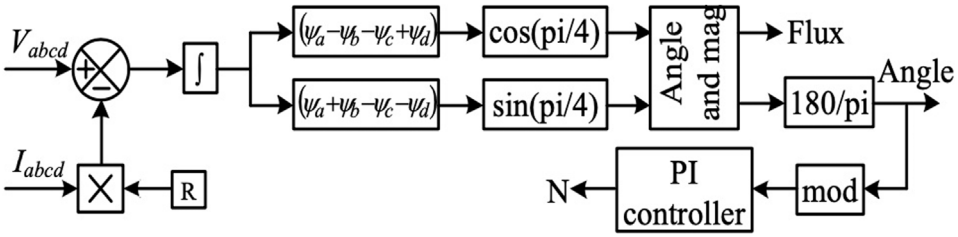

FIGURE 6
Implementation of the SMC in the proposed system.

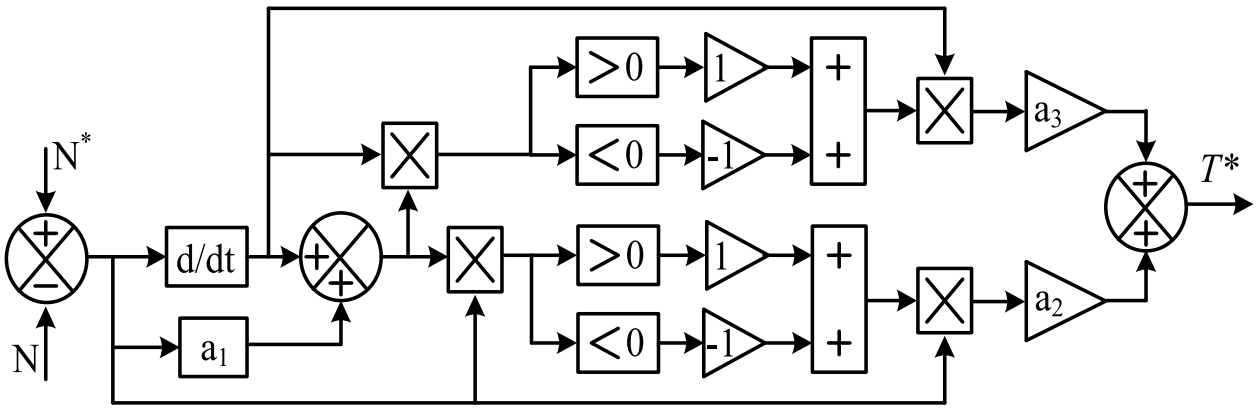

FIGURE 7
Block diagram of the sliding mode controller.

However, in (Rajanna and Kumar, 2021), the authors proposed a novel configuration with a lower number of switches for 6/4 pole machines. The proposed converter was modified to operate on an 8/6 pole machine, and its configuration is shown in Figure 4 The proposed converter consists of only five switches, making it a cost-effective converter compared to the conventional one. Moreover, the proposed configuration can also reduce the size of the overall system.

By comparison with the proposed converter in (Manne et al., 2020), one more switch was included, since the converter was designed to supply power to an 8/6 pole machine, which requires four legs for eight poles. However, the authors in (Kolluru and Kumar, 2021) proposed a converter for a generalized model for three legs. In the same manner, the number of switches can be increased to operate a higher number of pole machines (i.e., by increasingthe

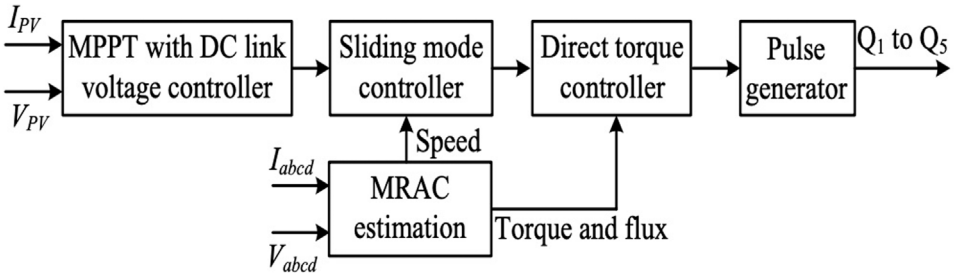

FIGURE 8
Pulse generator for the proposed converter.

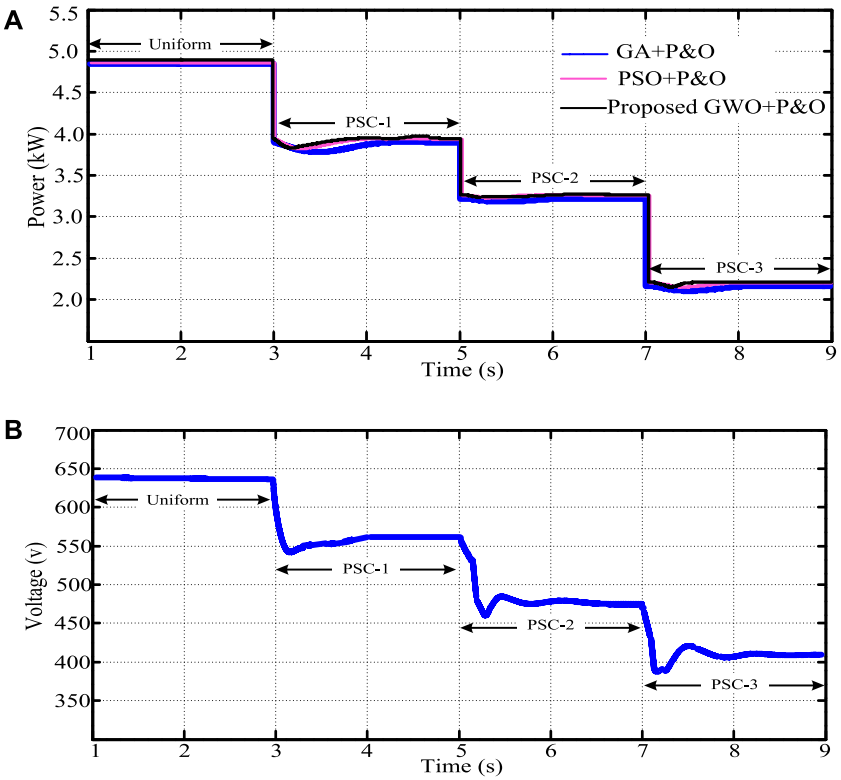

FIGURE 9
(A). Power, **(B)**. Actual DC link voltage (V_{dc}).

number of legs). This paper considered an 8/6 pole machine since it has the required torque capability for lifting water from 150 feet. Therefore, the converter proposed in (Kolluru and Kumar, 2021) was slightly modified in (Shanthi et al., 2021) to operate an 8/6 pole machine by adding one more switch without disrupting the complete topology. The space vector topology was implemented for the high-side switch asymmetric converter, with the required switching pattern listed in Table 3. The corresponding diodes are forward-biased when the currents of the corresponding inductors start to discharge.

3 SRM control

Figure 5A illustrates the basic MRAC block diagram (Ali et al., 2022; Mao et al., 2023), while Figure 5B illustrates the SRM motor

speed estimation (b). A target action from a reference mathematical model of the motor was compared with the output of the MRAC system. By tracking the error signal based on the PI controller, the parameters used to estimate the speed were updated. Figure 6 illustrates the block diagram for implementing SMC in the proposed system.

The amount of power available from PV determined the DC link voltage. Similarly, the speed of the motor was determined by the input power for a specific load torque, which was constant under stable conditions for a given depth of ground. The speed reference, which was calculated by comparing the DC link voltage with the reference voltage signal generated by the P and O algorithm, was matched to the projected motor speed using the MRAC model (i.e., Figure 6), and the required reference torque was calculated using the SMC (i.e., Figure 7). References (Manne et al., 2020; Kolluru and Kumar, 2021) implement the SMC The DTC achieved the required pulses for the high-side switch asymmetrical converter, as shown in Figure 8.

4 Simulation results and discussion

4.1 Performance under PSCs

The proposed control of WPS with the specifications in Tables 1, 2 was simulated using MATLAB/SIMULINK for partial shading conditions, changes in irradiance, and load changes. This section presents the simulation results for each condition and the performance of the proposed system. This study considered three patterns of solar irradiance to evaluate the performance of GA, PSO, and the proposed GWO, as indicated in Figure 9A. The DC link reference voltage was plotted using the proposed method, as shown in Figure 9B. The DC link voltage was adjusted by the POGWO algorithm to operate the PV system at the maximum power point.

4.2 Performance under changing irradiance

Considering a drop in the variation of solar irradiance by 250 W/m^2, the tracking performance for extracting maximum power is illustrated in Figure 10. By observing Figure 10, the performance of maximum power tracking is well with the proposed controller.

4.3 Speed, torque, and water discharge response

When the irradiance abruptly changed from maximum (1,000 W/m^2) to minimum (400 W/m^2) at t = 3.0 s, the system was put to thr test. As the irradiance suddenly dropped, the power available from the PV was also reduced. And DCLC provides a corresponding speed reference for motor MRAC can also calculate the SRM estimated speed When these two-speed signals are compared, the converter can receive matching pulses from the SMC. Figure 11 shows the corresponding speed response. The torque on the motor, on the other hand, remained constant, as shown in

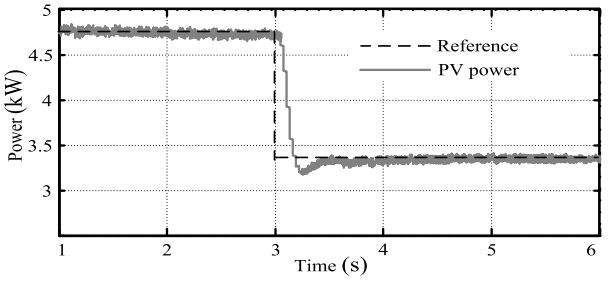

FIGURE 10
Performance of MPPT under changing irradiance.

Figure 12, which illustrates the comparable electromagnetic torque generated by the motor. Furthermore, as the motor speed reduced, the water flow through the pump was also reduced. Figure 13 illustrates the corresponding water discharge.

4.4 Speed response to irradiance changes

The WPS was tested under solar irradiance fluctuations between 900 W/m^2 and 650 W/m^2 at t = 1.5 s and again reaching 1,000 W/m^2 at t = 2.25 s. The corresponding reference speed and actual speed of the SRM are shown in Figure 14. The reference speed of the SRM motor was reduced while decreasing irradiance was used to reduce the DC link voltage. Therefore, the controller tried to follow the reference speed, resulting in low-speed operation. Again, the speed increased as the irradiance increased due to greater power availability, which is reflected in the higher DC link voltage.

4.5 Response when an additional pipe is introduced

Adding a new pipe to bring water from one area to another is a typical occurrence in WPS. WPS are generally made of HDPE, PVC, LDPE, and lateral pipes. The torque generated by the friction and external pressure acting on the water in the pipe grows in proportion to the length of the pipe.

Furthermore, if an extra pipe is added to a bore well, the torque applied to the motor will gradually rise until the water reaches the new outlet. In this circumstance, a 20-m pipe was used to transport water from the bore well outflow point to the new position, with the torque and water discharge shown in Figure 15. As the torque on the motor increased, the motor's speed also increased, but the power remained constant. As a result, when the pipe is horizontally connected to the land, the water discharge will remain constant. However, because of friction losses and external factors working against the motor's power/torque, it will be slightly reduced.

4.6 Input current of the SRM

The motor current is DC, but it will be pulsating DC The currents of the motor at 1,500 rpm are depicted in Figure 16 with proper pole representation. The currents in each phase will increase from

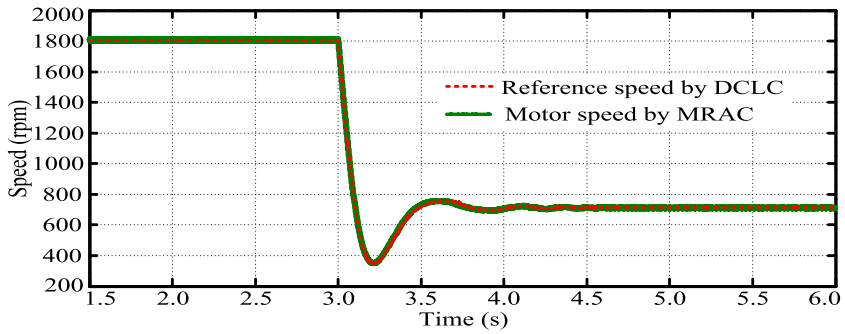

FIGURE 11
SRM rotor speed with DCLC and MRAC.

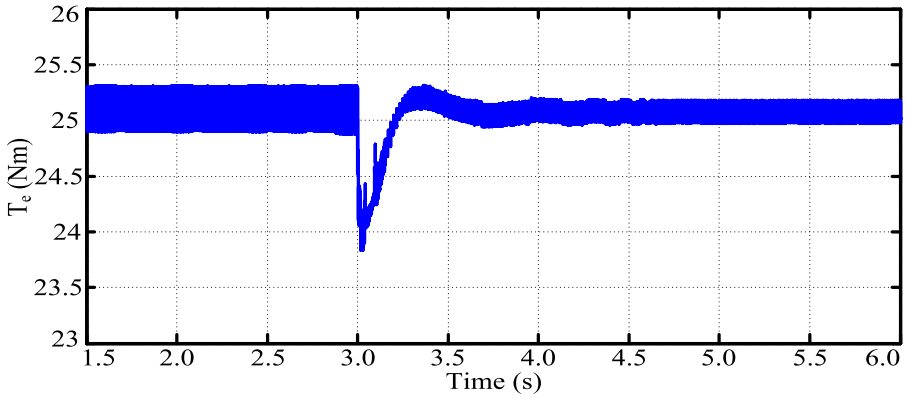

FIGURE 12
Electromagnetic torque response to changes in irradiance.

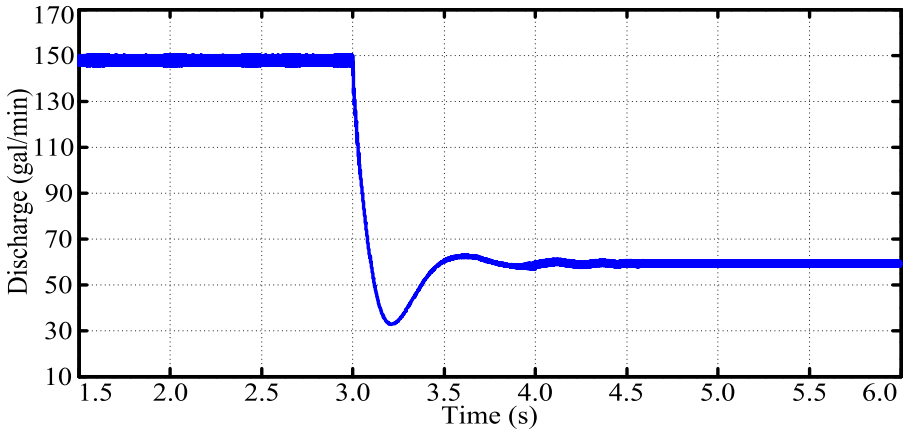

FIGURE 13
Water discharge during changes in irradiance.

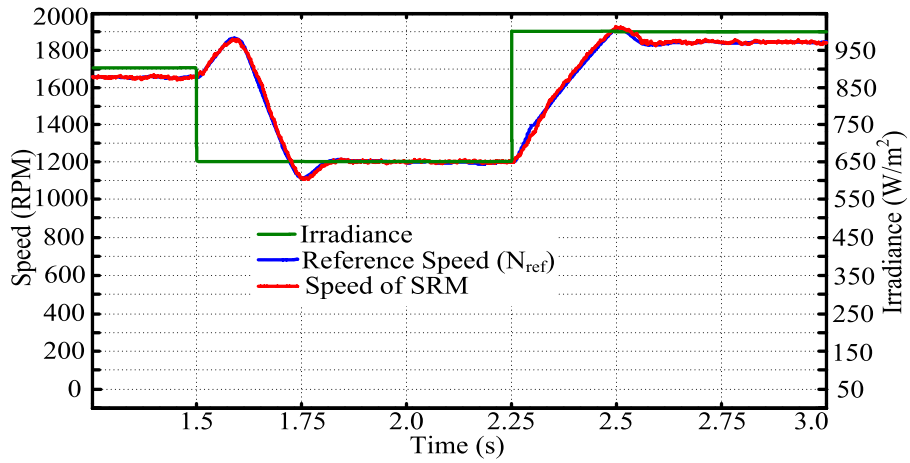

FIGURE 14
Speed response during changes in irradiance.

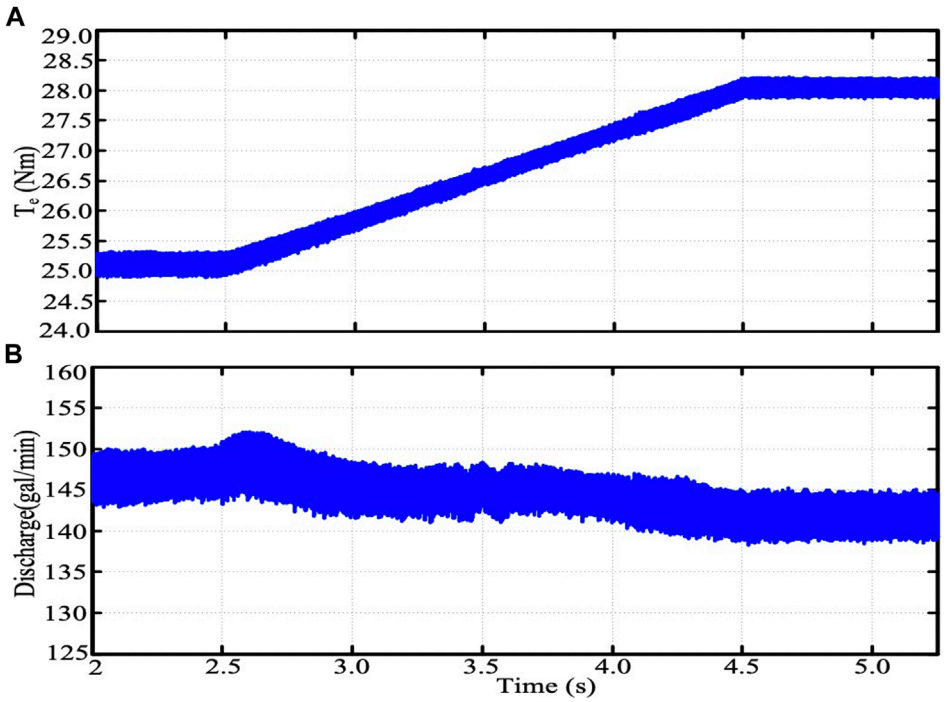

FIGURE 15
Torque and water discharge. **(A)** Electromagnetic torque **(B)** volume of water outflow for additional discharge pipe.

angle to angle as the corresponding switches are turned on. Similarly, the diodes will become forward-biased as the corresponding leg inductances start discharging, as shown in Table 2.

4.7 Comparison to existing methods

The simulation results demonstrate the accuracy and robustness of the proposed control structure in terms of MPP tracking, DC link regulation, and current control of the common high-side switch converter for WPS. In this section, the performance of the POGWO algorithm for MPPT and MRAC for SRM speed estimation in terms of the proposed control structure was compared with existing algorithms. It was observed that the proposed POGWO technique with a transient time of 0.3 s and efficiency of 99.99% gave a better dynamic response and accurate convergence in tracking MPP as compared to the PSO-assisted P&O (Mohanty et al., 2017) and GA-assisted P&O (Malla and N Bhende, 2014). The efficiency and transient time for tracking MPP are listed in Table 4.

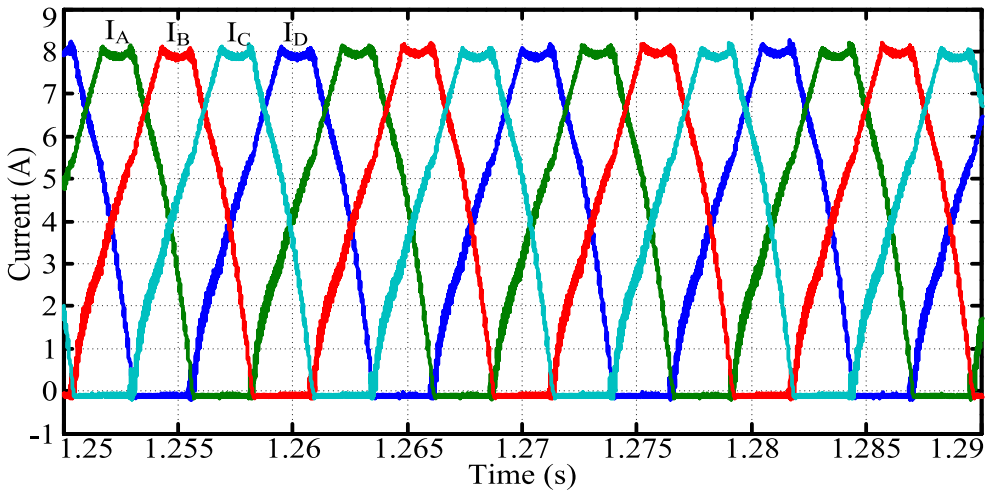

FIGURE 16
8/6 pole SRM input currents.

TABLE 4 Performance comparison.

Index	PSO (Mohanty et al., 2017)	GA (Malla and N Bhende, 2014)	Proposed system
Efficiency of MPPT	99.84%	99.91%	99.99%
Transient time for MPPT	0.35 s	0.32 s	0.3 s
Transient time for speed change under changes in irradiance	0.83 s	0.82 s	0.8 s

TABLE 5 Component size comparison.

Index	Two-stage asymmetric converter topology (Pradhan et al., 2020)	Proposed topology
No. of power switches	6	4
No. of power stages	2	1
Speed sensor	Required	Not required
MPP controller	Required	Not required

The speed command shifted to a new value as the irradiance changed. The transient time for tracking new speeds under a change in irradiance was also compared with existing algorithms. The proposed method showed robustness in tracking the new speed under changes in irradiance, as shown in Table 4. Although the improvements are small in magnitude, the consistency of the algorithm in tracking speed is comparable to the existing algorithms.

The proposed topology provided a reduction in the number of components, as shown in Table 5.

The sensorless speed estimation for SRM using MRAC accurately estimated the SRM speed with 98.9 percent accuracy, which is 98.5% for the sensorless speed estimation proposed in (Stonier et al., 2021). Changes in load due to water discharge with additional pipe (which is the typical case), proved the increment in torque provided by the motor to discharge the same amount of water. Thus, the proposed system is robust in terms of the dynamic response of MPP tracking and speed, efficient, and adaptive for current control under changes in load conditions.

5 Conclusion

Thus, a PV-powered and novel converter-fed SRM-based WPS was developed. The proposed model prioritized the use of WPS with SRM in conjunction with the proposed converter, considering a variety of practical issues such as the need for an additional pipe to transport water from one area to another. Single-stage power conversion and the integration of MPP into the drive converter control represent novel contributions. Also, the proposed MRAC for speed estimation was found to be efficient and accurate in speed estimation, with a 98.9% accuracy in speed

tracking. Extensive results validated the proposed POGWO strategy, with an accuracy of 99.99% in tracking MPP with a good transient time of 0.3 s. Also, speed commands and load changes were tracked within 0.8 s. Thus, the proposed work contributed to speed sensorless closed-loop control with a cost-effective power electronic interface for water pumping applications. In further studies, the proposed topology and control scheme would be modified to apply to multiple sources fed, such as the PV-grid and battery-based SRM pump drive.

Data availability statement

Publicly available datasets were analyzed in this study. This data can be found here: A Controller was developed.

Author contributions

MK, KM, ST, and CR contributed to conception and design of the study. CR, MA, and KM organized the database. MA, ST, and KM performed the statistical analysis. AK wrote the first draft of the manuscript. MK, KM, ST, and CR wrote sections of the manuscript. All authors contributed to the article and approved the submitted version.

Acknowledgments

The authors would like to acknowledge the support received from the Saudi Data and AI Authority (SDAIA) and King Fahd University of Petroleum and Minerals (KFUPM) under the SDAIA-KFUPM Joint Research Center for Artificial Intelligence Grant Nos JRC-AI-RFP-08, Dhahran 31261, KSA. Additionally, the authors would like to thank King Khalid University (KKU) for their financial support of this study.

Conflict of interest

The authors declare that the research was conducted in the absence of any commercial or financial relationships that could be construed as a potential conflict of interest.

Publisher's note

References

Abido, M. A., Sheraz Khalid, M., and Worku, Muhammed Y. (2015). An efficient ANFIS-based PI controller for maximum power point tracking of PV systems. *Arabian J. Sci. Eng.* 40, 2641–2651. doi:10.1007/s13369-015-1749-z

Abubakar, M., Renner, H., and Schürhuber, R. (2023). Development of a novel control scheme for grid-following converter under asymmetrical faults. *Energies* 16 (3), 1276. doi:10.3390/en16031276

Ali, N., Gao, Q., Sovička, P., Makyš, P., Štulrajter, M., and Ma, K. (2022). Power converter fault detection and isolation using high-frequency voltage injection in switched reluctance motor drives for automotive applications. *IEEE J. Emerg. Sel. Top. Power Electron.* 10 (3), 3395–3408. doi:10.1109/JESTPE.2020.3022575

de Oliveira, T. H., Antuña, A. L., Aller, D. G., Lamar, D. G., and Arias, M. (2023). Double bus provider asymmetrical half bridge converter with a resonant DCX-derived auxiliary circuit to supply a LED-based VLC postregulator. *IEEE Trans. Industrial Electron.* 70 (8), 7845–7854. doi:10.1109/TIE.2022.3227231

Goud, B. S., and Reddy, C. R. (2020). Essentials for grid integration of hybrid renewable energy systems: A brief review. *Int. J. Renew. Energy Res. (IJRER)* 10 (2), 813–830.

Haq, S., Biswas, S. P., Hosain, M. K., Rahman, M. A., Islam, M. R., Elavarasan, R. M., et al. (2023). A modified PWM scheme to improve the power quality of NPC inverter based solar PV fed induction motor drive for water pumping. *IEEE Trans. Industry Appl.* 59, 3019–3030. doi:10.1109/TIA.2023.3245590

Ibrahim, M. N., Rezk, H., Al-Dhaifallah, M., and Sergeant, P. (2019). Solar array fed synchronous reluctance motor driven water pump: An improved performance under partial shading conditions. *IEEE Access* 7, 77100–77115. doi:10.1109/access.2019.2922358

Jayachandran, M., Reddy, C. R., Padmanaban, S., and Milyani, A. H. (2021). Operational planning steps in smart electric power delivery system. *Sci. Rep.* 11 (1), 17250. doi:10.1038/s41598-021-96769-8

Kashif, M., and Singh, B. (2023). Reduced-sensor-based multistage model reference adaptive control of PV-fed PMSM drive for water pump. *IEEE Trans. Industrial Electron.* 70 (4), 3782–3792. doi:10.1109/TIE.2022.3176279

Khalid, Muhammad, and Savkin, Andrey V. (2010). A model predictive control approach to the problem of wind power smoothing with controlled battery storage. *Renew. Energy* 35 (7), 1520–1526. doi:10.1016/j.renene.2009.11.030

Kolluru, A. K., and Kumar, M. K. (2021). Artificial neural network vector controlled common high-side switch asymmetric converter fed switched reluctance motor drive. *Indonesian J. Electr. Eng. Comput. Sci.* 24 (2), 697–703. doi:10.11591/ijeecs.v24.i2.pp697-703

Kumar, R., and Singh, B. (2017). Single stage solar PV fed brushless DC motor driven water pump. *IEEE J. Emerg. Sel. Top. Power Electron.* 5 (3), 1377–1385. doi:10.1109/jestpe.2017.2699918

Kumar, R., and Singh, B. (2019). Grid interactive solar PV-based water pumping using BLDC motor drive. *IEEE Trans. Industry Appl.* 55 (5), 5153–5165. doi:10.1109/tia.2019.2928286

Kumaraswamy, A., Bhattacharya, A., and Sadhu, P. K. (2023). Dual output and dual-frequency resonant inverter-based induction heating using ADC control. *IETE J. Res.*, 1–13. doi:10.1080/03772063.2023.2175047

Li, Z., Tang, B., Song, Q., Gou, L., Zhao, B., Jia, N., et al. (2023). Low-cost and compact asymmetrical unidirectional-current modular multilevel converters. *IEEE Trans. Power Electron.* 38 (3), 3398–3411. doi:10.1109/TPEL.2022.3225861

Malla, S. G., and N Bhende, C. (2014). Enhanced operation of stand-alone "Photovoltaic-Diesel Generator-Battery" system". *Elsevier Electr. Power Syst. Res.* 107, 250–257. doi:10.1016/j.epsr.2013.10.009

Manne, B., Kumar, M. K., and &Akuru, U. B. (2020). Design and performance assessment of a small-scale ferrite-PM flux reversal wind generator. *Energies* 13 (21), 5565. doi:10.3390/en13215565

Mao, H., Jiang, H., Ran, L., Hu, J., Qiu, G., Wei, J., et al. (2023). An asymmetrical power module design for modular multilevel converter with unidirectional power flow. *IEEE Trans. Power Electron.* 38 (1), 1092–1103. doi:10.1109/TPEL.2022.3198859

Mishra, Anjanee Kumar, and Singh, Bhim (2018). Design of cost effective solar PV powered SRM driven agriculture pump using modified buck-boost converter. *Int. J. Emerg. Electr. Power Syst.* 19 (5), 20180028. doi:10.1515/ijeeps-2018-0028

Mishra, S., Karthikeyan, A., Varsha, S., and Perumal, B. V. (2020). Standalone single stage PV-fed reduced switch inverter based PMSM for water pumping application. *IEEE Trans. Industry Appl.* 56 (6), 6526–6535. doi:10.1109/tia.2020.3023870

Mohanty, S., Subudhi, B., and Ray, P. K. (2017). A grey wolf-assisted perturb & observe MPPT algorithm for a PV system. *IEEE Trans. Sustain. Energy* 32 (1), 340–347. doi:10.1109/tec.2016.2633722

Murshid, S., and Singh, B. (2018). A novel vector control scheme for PMSM driven encoder-less solar water pumping system. In Proceedings: IECON 2018 - 44th Annual

Conference of the IEEE Industrial Electronics Society. 1619–1624. Washington, DC, USA. October 2018, doi:10.1109/IECON.2018.8592681

Murshid, S., and Singh, B. (2019). Implementation of PMSM drive for a solar water pumping system. *IEEE Trans. Industry Appl.* 55 (5), 4956–4964. doi:10.1109/tia.2019.2924401

Narale, Pradip, and Singh Rathore, Narendra (2015). *Solar water pumping system for agriculture*". Energética India: Department of Renewable Energy Engineering, MP University of Agriculture and Technology.

Pourfarrokh, S., Adabi, J., and Zare, F. (2023). A novel multilevel inverter with self-balancing capability of capacitors voltage; structure, modulation, and operation. *IEEE J. Emerg. Sel. Top. Power Electron.* 11 (2), 1854–1864. doi:10.1109/JESTPE.2022.3222344

Pradhan, C., Senapati, M. K., Malla, S. G., Nayak, P. K., and Gjengedal, T. (2020). Coordinated power management and control of standalone PV-hybrid system with modified IWO-based MPPT. *IEEE Syst. J. early access* 15, 3585–3596. doi:10.1109/jsyst.2020.3020275

Rajanna, B. V., and Kumar, M. K. (2021). Chopper-based control circuit for BESS integration in solar PV grids. *Energies* 14 (6), 1530. doi:10.3390/en14061530

Ramulu, C., Karampuri, R., Jain, S., Sanjeevikumar, P., and Blaabjerg, F. (2018). Dual solar photovoltaic fed three-phase open-end winding induction motor drive for water pumping system application. *Electr. Power Components Syst.* 46, 1896–1911. doi:10.1080/15325008.2018.1520324

Ríos-Castro, D., Pérez-Estévez, D., and Doval-Gandoy, J. (2023). AC-voltage controller for grid-forming converters. *IEEE Trans. Power Electron.* 38 (4), 4529–4543. doi:10.1109/TPEL.2022.3233137

Sagvand, F., Siahbalaee, J., and Koochaki, A. (2023). An asymmetrical 19-level inverter with a reduced number of switches and capacitors. *Electron. Switz.* 12 (2), 338. doi:10.3390/electronics12020338

Sen, A., and Singh, B. (2021). Peak current detection starting based position sensorless control of BLDC motor drive for PV array fed irrigation pump. *IEEE Trans. Industry Appl.* 57 (3), 2569–2577. doi:10.1109/TIA.2021.3066831

Shanthi, T., Prabha, S. U., and Sundaramoorthy, K. (2021). Non-isolated n-stage high step-up DC-DC converter for low voltage DC source integration. *IEEE Trans. Energy Convers.* 36 (3), 1625–1634. doi:10.1109/TEC.2021.3050421

Shukla, Saurabh, and Singh, Bhim (2019). Reduced-sensor-based PV array-fed direct torque control induction motor drive for water pumping. *IEEE Trans. Power Electron.* 34 (6), 5400–5415. doi:10.1109/tpel.2018.2868509

Shukla, S., and Singh, B. (2020). Single-stage PV-grid interactive induction motor drive with improved flux estimation technique for water pumping with reduced sensors. *IEEE Trans. Power Electron.* 35 (12), 12988–12999. doi:10.1109/tpel.2020.2990833

Sir, K., Hao, Z., Yu, Q., Cao, X., Deng, X., and Shen, X. (2020). An improved direct torque control for a single-winding bearingless switched reluctance motor. *IEEE Trans. Energy Convers.* 35 (3), 1381–1393. doi:10.1109/TEC.2020.2988549

Stonier, A. A., Murugesan, S., Samikannu, R., Krishnamoorthy, V., Subburaj, S. K., Chinnaraj, G., et al. (2021). Fuzzy logic control for solar PV fed modular multilevel inverter towards marine water pumping applications. *IEEE Access* 9, 88524–88534. doi:10.1109/ACCESS.2021.3090254

Sundareswaran, K., Kumar, V., and Palani, S. (2015). Application of a combined particle swarm optimization and perturb and observe method for MPPT in PV systems under partial shading conditions. *Renew. Energy* 75, 308–317. doi:10.1016/j.renene.2014.09.044

Thumu, Raghu, Harinadha Reddy, Kadapa, and Rami Reddy, Chilakala (2021). Unified power flow controller in grid-connected hybrid renewable energy system for power flow control using an elitist control strategy. *Trans. Inst. Meas. Control* 43 (1), 228–247. doi:10.1177/0142331220957890

Varshney, A., Sharma, U., and Singh, B. (2021). An intelligent grid integrated solar PV array fed RSM drive-based water pumping system. *IEEE Trans. Industry Appl.* 57 (2), 1818–1829. doi:10.1109/TIA.2020.3045952

Yan, N., Cao, X., and Deng, Z. (2019). Direct torque control for switched reluctance motor to obtain high torque-ampere ratio. *IEEE Trans. Industrial Electron.* 66 (7), 5144–5152. doi:10.1109/TIE.2018.2870355